Journal of Solid State Electrochemistry (2022) 26:2805–2815
https://doi.org/10.1007/s10008-022-05281-0

ORIGINAL PAPER

The electrochemical behaviour of butyltrimethylammonium bis(trifluoromethylsulfonyl)imide at negatively polarised aluminium electrode studied by in situ soft X-ray photoelectron spectroscopy, electrochemical impedance spectroscopy and cyclic voltammetry techniques

Jaanus Kruusma[1] · Tanel Käämbre[2] · Arvo Tõnisoo[2] · Vambola Kisand[2] · Karmen Lust[1] · Enn Lust[1]

Received: 27 June 2022 / Revised: 22 August 2022 / Accepted: 23 August 2022 / Published online: 9 September 2022

Abstract

The in situ X-ray photoelectron spectroscopy data indicate that butyltrimethylammonium bis(trifluoromethylsulfonyl) imide (N4111(TFSI)) adsorbs strongly within the potential range $-3.25\ V < E < -2.25\ V$ and specifically at $E < -3.25$ V (vs. Ag-QRE) at the Al electrode. Strong adsorption of the intermediates of N4111(TFSI) electrochemical decomposition was observed in electrochemical impedance spectroscopy and cyclic voltammetry measurements. At $E < -4.25$ V (vs. Ag-QRE), very intensive electrochemical reduction of N4111(TFSI) took place at the Al electrode giving gaseous products. In the potential range from − 2.25 to 0.00 V (vs. Ag-QRE), non-specific adsorption of N4111(TFSI) exists et al. surface.

Keywords Room-temperature ionic liquid · X-ray photoelectron spectroscopy · Cyclic voltammetry · Electrochemical impedance spectroscopy · Aluminium current collector

Introduction

Butyltrimethylammonium bis(trifluoromethylsulfonyl) imide (N4111(TFSI), CAS number 945715–39-9) is one of the quaternary ammonium-based room-temperature ionic liquids (RTILs) being suggested to use as an electrolyte in the supercapacitors and electrochemical power sources due to its very wide region of ideal polarizability at the carbon electrode—electrolyte interface [1, 2]. However, it has been predicted that N4111(TFSI) starts to electroreduce at glassy carbon electrode at $E = -3.35$ V vs. Fc/Fc^+ [3] (ca. −2.9 V vs. Ag/Ag^+), and the linear fit method has given a cathodic stability limit for various quaternary ammonium cations at glassy carbon electrode at around $E = -3.4$ V vs. Ag/Ag^+ [2]. On the other hand, Howlett et al. have reported the electrochemical instability of the $TFSI^-$ anions as early as at $E < -2.0$ V vs. Fe/Fe^+ [4]. Therefore, the question about the initial potential for electrochemical reduction of $N4111^+$ cations and $TFSI^-$ anions at the carbon and metal electrodes remains.

Al is a commonly used inexpensive material for the production of the current collectors in supercapacitors, reflecting its great importance in technology [5–7]. Therefore, it is essential that Al, as the current collector, is in direct contact with the electrolyte solution inside a supercapacitor [8–10]. Thus, it is essential to investigate and analyse the electrochemical processes at polarised Al current collectors, including Al passivation by the electrolyte and the re-activation at more negative potentials, adsorption and desorption of the electrolyte components and reaction intermediates, etc. In this work, the properties of the negatively polarised Al electrode in N4111(TFSI) were studied by in situ X-ray photoelectron spectroscopy (XPS), electrochemical impedance spectroscopy (EIS) and cyclic voltammetry (CV) methods.

✉ Enn Lust
enn.lust@ut.ee

[1] Institute of Chemistry, University of Tartu, Ravila 14a, 50411 Tartu, Estonia

[2] Institute of Physics, University of Tartu, W. Ostwaldi 1, 50411 Tartu, Estonia

Experimental

Materials

The Al material was used as a working electrode (WE) in the electrochemical measurements and as an electrochemically polarised support for the low energy ("soft") X-ray photoelectron spectroscopy (XPS) studies of N4111(TFSI). This Al material has also been applied as a current collector in a model electrochemical double-layer capacitor containing molybdenum carbide derived high surface area micro-mesoporous carbon electrodes, the electrochemical and spectroscopic properties of which have been previously described [11, 12]. The Al was mechanically cleaned and polished by Buehler Carbimet® (SiC) grit 600 polishing paper and then washed with acetone (Honeywell/Riedel–de Haen, for HPLC, ≥ 99.8%) before the wetting with N4111(TFSI) and following analysis. The purity of the pre-cleaned Al current collector was determined by X-ray fluorescence spectroscopy, and the presence of 96.4% (w/w) Al, 1.9% (w/w) C and 1.7% (w/w) O at the material surface was indicated. Platinum gauze (with an apparent area of ca. 2 cm^2 and grid size 100 mesh, purity 99.9% (w/w)) as the counter electrode (CE) and a silver wire as the quasireference electrode (Ag-QRE) (next to WE) were located in the quartz electrochemical cell filled with 1 ml N4111(TFSI) [13]. Therefore, all electrochemical potentials (E) noted in the text are given in the reference to Ag-QRE.

N4111(TFSI) (>99.5%, Iolitec), containing 80 ppm water and less than 50 ppm halides (according to manufacturer's certificate), was dried further at 100 °C and 10 kPa for 20 h. The three-electrode electrochemical system filled with N4111(TFSI) was degassed in the XPS sample preparation chamber for 12 h at 22 °C and $p = 5 \times 10^{-5}$ Pa before the in situ XPS measurements.

Equipment and data analysis

The CV and EIS studies of the N4111(TFSI) | Al interface were performed in the mBraun Ar-filled glovebox ($p = 101$ kPa) containing less than 0.1 ppm water and oxygen. Reference 3000 (Gamry Instruments) and SP-300 (Bio-Logic SAS) potentiostats were used to record electrochemical data and to polarise the Al electrode during the in situ XPS and MS measurements. The values of the series and parallel resistances were calculated by fitting the calculated impedance spectra to the experimental Nyquist plots using a model combination circuit where the resistor was connected in series with the parallel combination of the second resistor and the constant phase element (Scheme 1). Autolab NOVA 1.11 software was used for the calculation of theoretical spectra and fitting of calculated data to the experimental ones.

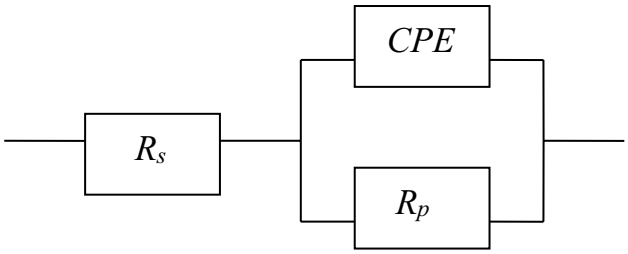

Scheme 1 The equivalent scheme (model) used to describe the electrochemical behaviour of the N4111(TFSI) | Al interface. R_s series resistance, R_p parallel resistance and *CPE* constant phase element

The in situ XPS measurements were conducted in the high vacuum conditions ($p = 0.08 \ldots 1 \times 10^{-4}$ Pa) at the synchrotron initiated adjustable energy X-ray beamline FlexPES low density matter branch end-station (Max IV laboratory, Lund University, Sweden). The following excitation photon energies were used: for C 1 s –400.0 eV, for N 1 s –500.0 eV, for O 1 s –650.0 eV, for F 1 s –800.0 eV and for S 2p and Al 2p –270 eV. XPS data analysis and binding energy (*BE*) spectra fittings were performed using CasaXPS software (ver. 2.3.19). The C 1 s XPS spectra were fitted using a combined Gaussian-Lorentz function with the ratio 70:30, respectively. For the calibration of the *BE* scale, the *BE* of the C 1 s electrons originating from the aliphatic carbon atoms in the butyl chain (i.e. not connected with the ammonium nitrogen atom and having sp^3 electronic configuration) of $N4111^+$ cation located at the non-polarised Al WE was fixed at 285.0 eV [14]. This method enabled to calibrate the measured XPS spectra internally. For precise fitting and the extraction of the C 1 s *BE* peaks, the two-peak model was selected for the analysis of the $N4111^+$ cation core electron energies.

The N 1 s, O 1 s, F 1 s and S 2p X-ray photoelectron (PE) spectra were fitted using the same combination ratio of the Gaussian-Lorentz function as described for C 1 s XPS, leaving the FWHM and peak positions free. Later the obtained individual peak *BE*s were corrected according to the *BE* of the aliphatic carbon measured for different fixed potentials.

All investigations were performed at room temperature (22 °C).

Results and discussion

In situ XPS measurements

The shapes of the C 1 s, N 1 s, O 1 s, F 1 s and S 2p X-ray photoelectron (PE) spectra were stable throughout the potential range investigated: from −4.25 to 0.00 V (Fig. 1).

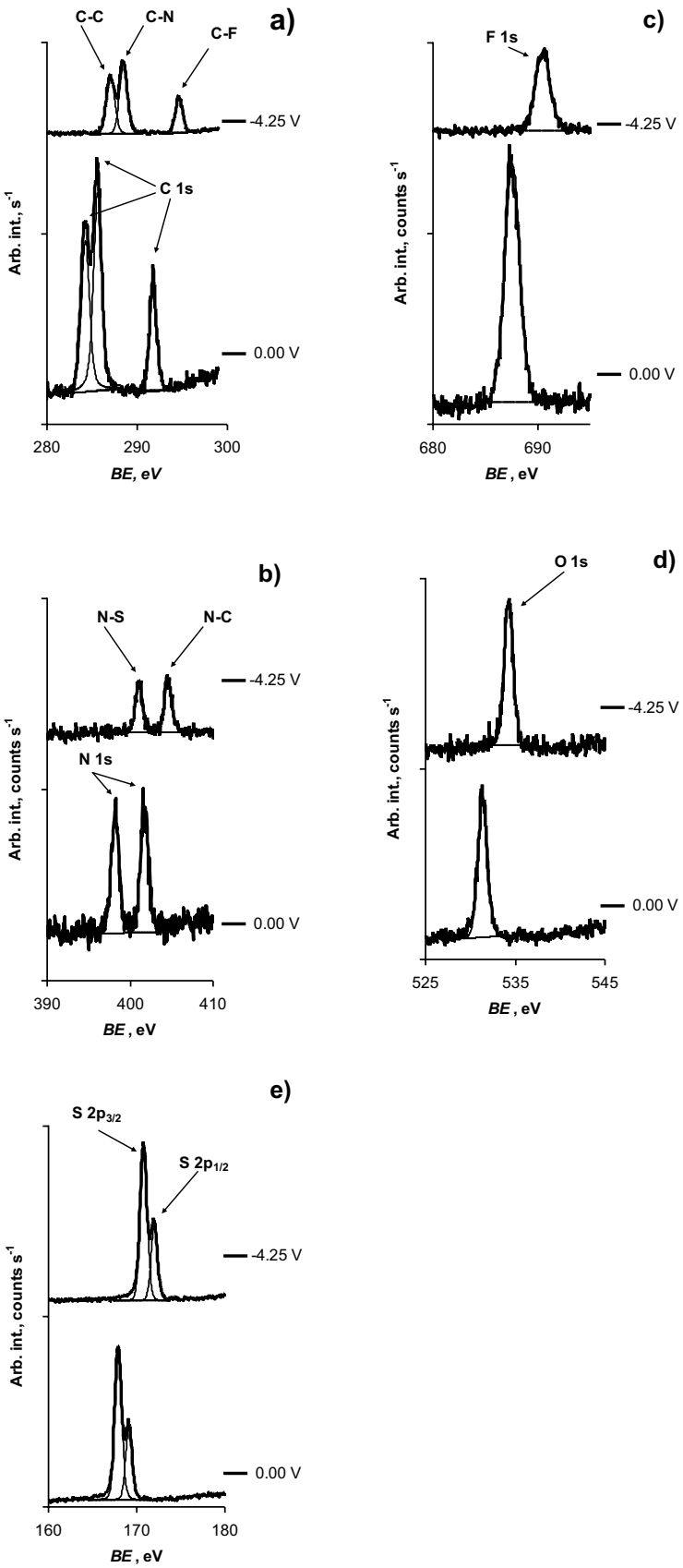

Fig. 1 In situ XPS spectra for Al electrode at various potentials marked in the figures: **a** for C 1 s, tick mark labels $1.2{\cdot}10^6$ counts s^{-1}; **b** for N 1 s, tick mark labels $3{\cdot}10^5$ counts s^{-1}; **c** for O 1 s, tick mark labels $3{\cdot}10^5$ counts s^{-1}; **d** for S 2p, tick mark labels $3{\cdot}10^6$ counts s^{-1}; and **e** for F 1 s, tick mark labels $2.1{\cdot}10^5$ counts s^{-1}

Binding energies of the inner core electrons, corresponding to the photoelectron peaks in Fig. 1, are presented in Supporting Information STable 1. Application of more negative potentials than $E = -4.25$ V was impossible due to the increasingly rapid release of gaseous products. Stability of the shape of the PE peaks indicates that gaseous or insoluble products formed et al. WE. dBE vs. dE relationships, constructed using collected and fitted C 1 s, N 1 s, O 1 s, F 1 s and S 2p X-ray PE spectra data, indicate that N4111(TFSI) adsorbed non-specifically et al. WE at $E > -2.25$ V, $dBE \cdot dE^{-1} = -1.0$ eV V^{-1}, as for all elements investigated. At more negative potentials $E < -3.25$ V strong adsorption ($dBE \cdot dE^{-1} \approx -0.15$ eV V^{-1}) is possible for most of the elements investigated (STable 1 and Supporting Information Figs. (SFigs. 1, 2, 3, 4, 5, 6, 7, and 8). Within the potential region -3.25 V $< E < -2.25$ V, a smooth change in the slope of the dBE vs. dE plot takes place having an average value of $dBE \cdot dE^{-1} \approx -0.6$ eV V^{-1} for inner core electrons of all N4111(TFSI) component atoms (STable 1 and SFigs. 1, 2, 3, 4, 5, 6, 7, and 8) indicating possible exchange of the adsorption nature of N4111(TFSI) in this potential range and very slow surface film formation. Thus, the in situ XPS data obtained are in a very good correlation with the Campana et al. [15] in situ atomic force microscopy measurement information collected for tetraethylammonium tetrafluoroborate solution in propylene carbonate at highly oriented pyrolytic graphite electrode.

Information collected in CV measurements

The CV data, performed within the potential range from 0.00 to −3.00 V and reverse at the potential sweep rate $v = 1.0$ mV s^{-1}, indicate the start of an electroreduction process at $E \leq -2.25$ V (Fig. 2, grey line). The reduction process has the highest speed at the most negative potential applied ($E = -3.00$ V) and starts to reduce again as the potential is increased. However, Fig. 2 shows a hysteresis loop indicating the presence of adsorption–desorption processes within the potential range -3.00 V $< E < -1.80$ V (Fig. 2, grey line). It should be also noted that no hysteresis loop formed in the CV measured in a narrower potential range from 0.00 to −2.50 V (Fig. 2, black line). Thus, it seems that strong adsorption of N4111(TFSI) takes place only at $E < -2.50$ V.

CV measurements over even wider ranges of potential, i.e. potential changes from 0.00 to −3.50 V, 0.00 to −4.00 V and from 0.00 to −5.00 V and reverse, indicate significant activation of the Al surface as the reduction current starts to increase already at ca. $E < -1.0$ V (Fig. 3a, b). It is unlikely that the residual water began suddenly to reduce at this potential, as this process should to be notable already in previous CV sweeps with less negative ending potentials (Fig. 2). Thus, we propose that at more negative potential than $E = -1.0$ V, the electrocatalytic reduction of N4111(TFSI) is possible at previously electrochemically activated Al electrode at $E < -3.0$ V. This increased electrochemical activity of

Fig. 3 Cyclic voltammograms (CV) measured within the potential range from 0.00 V to the forward sweep end-potentials (indicated in the figure) and reverse at the potential sweep rate of 1.00 mV s^{-1} (**a**). Enlargement of Fig. 1a shows the behaviour of the CV sweeps for low intensity electrochemical processes (**b**). The second CV sweeps are presented

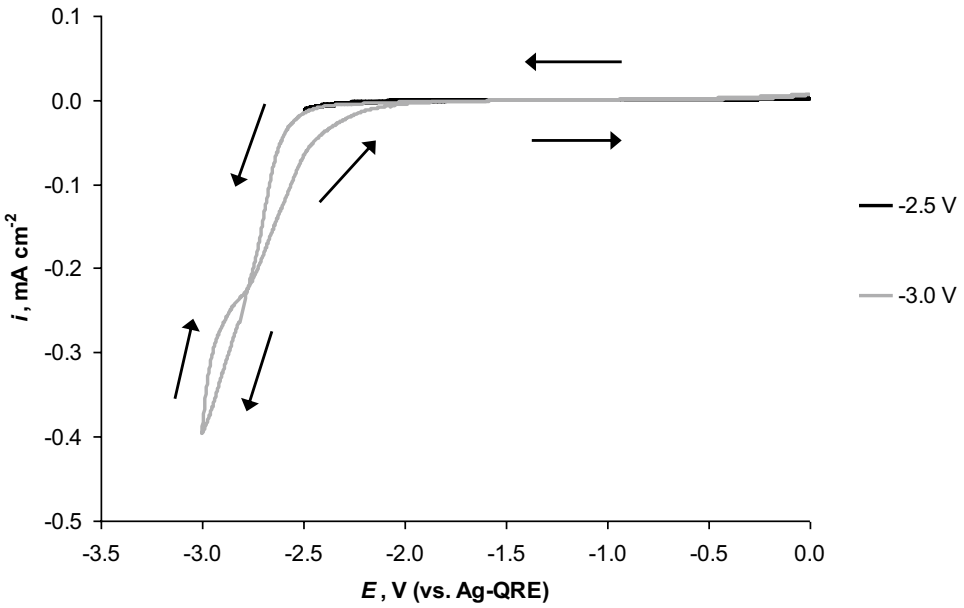

Fig. 2 Cyclic voltammogram (CV) measured within the potential range from 0.00 to −2.50 V (black line) and 0.00 to −3.00 V (grey line) at the potential sweep rate of 1.0 mV s^{-1}. The second forward and reverse CV sweeps are presented

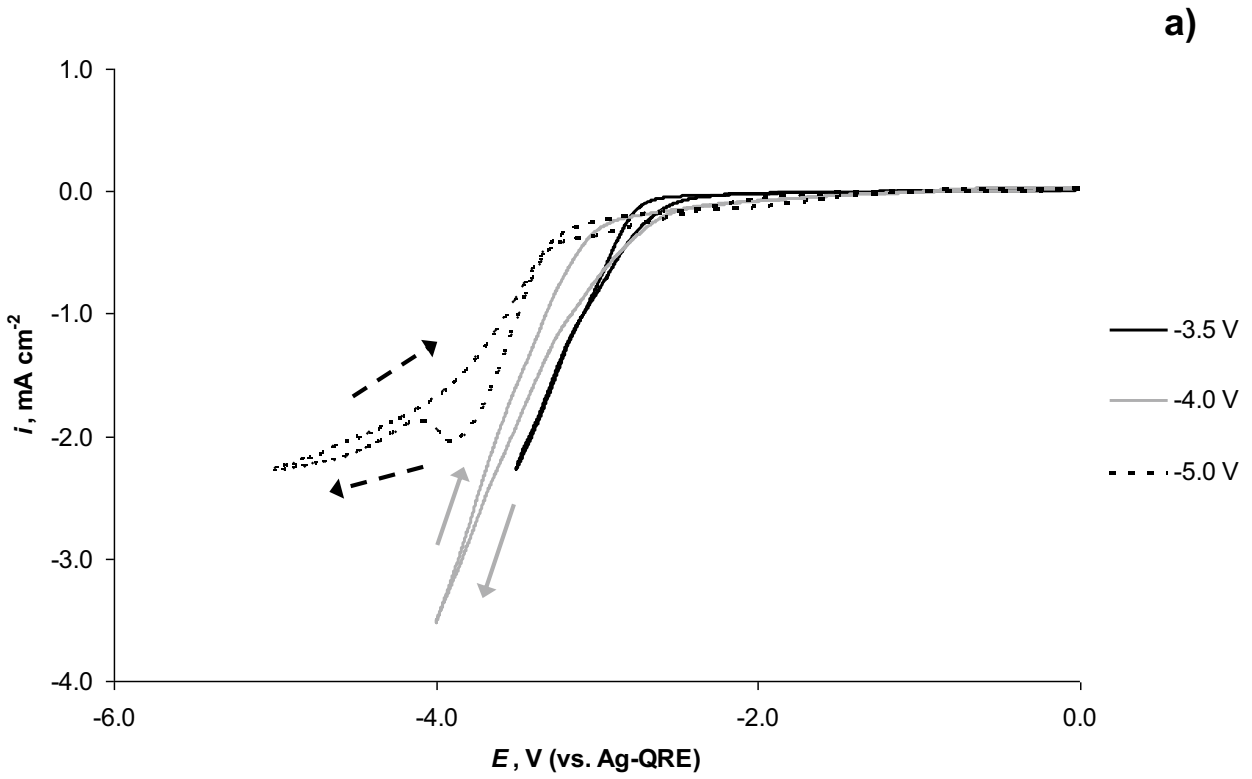
a)
1.0
0.0
-1.0
-2.0
-3.0
-4.0
i, mA cm-2
-6.0
-4.0
-2.0
0.0
E, V (vs. Ag-QRE)
-3.5 V
-4.0 V
-5.0 V

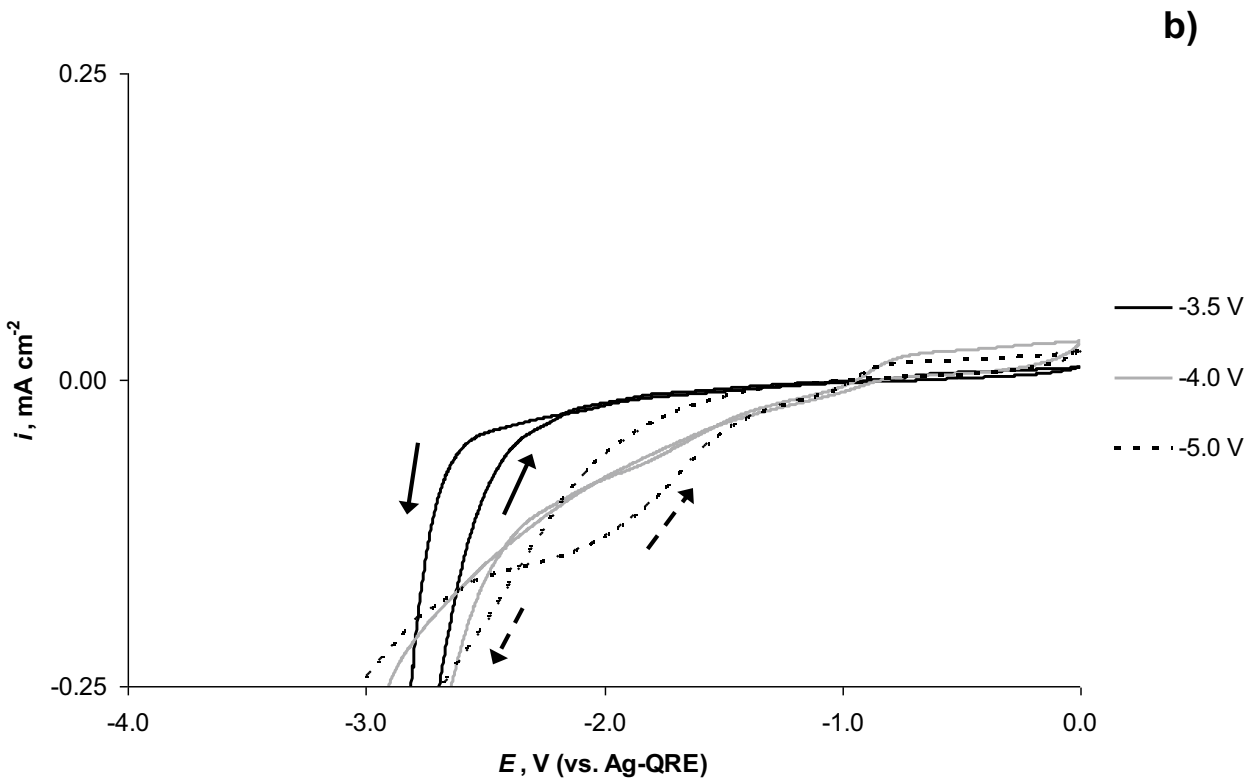
b)
0.25
0.00
-0.25
i, mA cm-2
-4.0
-3.0
-2.0
-1.0
0.0
E, V (vs. Ag-QRE)
-3.5 V
-4.0 V
-5.0 V

the N4111(TFSI) | Al system relates to the cleaning of the Al surface and very strong adsorption of N4111(TFSI) at the Al electrode, notable from the dBE vs. dE data obtained at $E < -3.25$ V (STable 1). Additionally, a small electroreduction peak formed at $E = -3.9$ V in the CV measured within the potential range from 0.00 to −5.00 V and reverse (Fig. 3a).

Information collected from the potentiostatic EIS measurements

The information was collected within the modulation frequency (ν) range from 300 kHz to 5 mHz with the application of the modulation amplitude of 5 mV to measure the EIS data in the potentiostatic mode. The Nyquist plots measured are presented in Fig. 4. Within the potential range from −0.80 to 0.00 V, the impedance imaginary part vs. impedance real part (-Z" vs. Z') relationships are almost straight lines and have very high -Z" vs. Z' values at very low frequencies (Fig. 4a). This indicates the absence of faradic processes and marks that the Al surface behaves nearly like an ideal passivated (so-called blocked) electrode (capacitor) having the most ideal capacitor-like behaviour at $E = -0.50$ V. At $E \leq -0.90$ V, the slope of the Nyquist plots starts slowly to reduce and bend. Parallel to that, the values of -Z" start to reduce indicating the start of very slow electrochemical processes. The log |-Z|" vs. log ν plots are straight lines with the slope of −0.91 (Ω cm^2 s) within the potential range -1.30 V $< E < 0.00$ V and −2.3 (Hz) < log ν < 2.0 (Hz) (SFig. 9). At $E = -1.90$ V, an arc seems to be formed (Fig. 4a) and the log |-Z"| vs. log ν plot straight line starts to deviate from linear dependence at log $\nu < -1.3$ (Hz) (SFig. 9). Stepwise increase of the negative potential of the Al electrode leads to more curved Nyquist plots, and from a potential of −2.20 V, the semi-circles form (Fig. 4b). Parallel to that, the maxima in the log |-Z"| vs. log ν plot form as well (SFig. 9), moving toward higher modulation frequencies, and the slope of the log |-Z"| vs. log ν plots reduces (dlog |-Z"| · (dlog ν)$^{-1} = -0.82$ (Ω cm^2 s) at $E = -2.50$ V and 0.43 (Hz) < log ν < 2.55 (Hz)), thus, indicating the acceleration of the mixed-kinetic electroreduction of N4111(TFSI) (i.e. slow adsorption and faradic charge transfer steps) (SFig. 9).

The formation of the semi-circle at $E \leq -2.20$ V (Fig. 4b) overlaps with the reduction of the slope of the dBE vs. dE relationships to −0.6 eV V^{-1} for the elements composing N4111(TFSI) at $E < -2.25$ V (STable 1), indicating the specific adsorption with partial charge transfer of the RTIL at the Al surface. The formation of two semi-circles in the Nyquist plots at $E < -2.70$ V (Fig. 4c) is overlapping with the reduction of the slope of the dBE vs. dE relationship to −0.1 eV V^{-1}, indicating the strong interaction of N4111(TFSI) with Al surface. Parallel to the changes in the shape of the Nyquist plots, the sizes of the semi-circles reduce parallel with the reduction of the Al electrode potential, reflecting the remarkable increase in the speed of the charge transfer processes at the N4111(TFSI) | Al interface (Figs. 2, 3a and 4b, c). Unfortunately, the N4111(TFSI) | Al interface became instable at $E < 3.30$ V, and thus, it was impossible to analyse the EIS data collected at more negative potentials.

The series capacitances (C_s), measured at the EIS modulation frequency $\nu = 0.10$ Hz and calculated as described in Refs. [9, 16], had very stable values from $E = 0.00$ to −2.00 V. At more negative potentials, C_s values begun to increase gradually. Very steep increase of the C_s values started at $E < -2.4$ V, when a first capacitance peak formed at $E = -2.60$ V ($C_s = 40$ mF cm^{-2}), followed by the second C_s peak at $E = -2.90$ V ($C_s = 40$ mF cm^{-2}) (Fig. 5a). After that the C_s values stabilised at $C_s = 30$ mF cm^{-2} and $E = -3.20$ V (Fig. 5a). The parallel capacitance (C_p) values, measured at the modulation frequency $\nu = 0.10$ Hz and calculated as in Ref. [16], show at $E > -2.4$ V very similar trend as for C_s values (Fig. 5a). At $E < -2.90$ V the C_p increased continuously up to $C_p = 0.9$ mF cm^{-2} at $E = -3.20$ V (Fig. 5a).

The ratio of $C_p \cdot C_s^{-1}$ being nearly unity (calculated at $\nu = 0.1$ Hz) is an indicator of the ideal polarisability of the electrochemical system investigated (i.e. of N4111(TFSI) | Al interface) [16], having the closest values to unity ($C_p \cdot C_s^{-1} = 0.97$) within the potential range from $E = 0.00$ to −1.20 V (Fig. 5b). At more negative potentials, the $C_p \cdot C_s^{-1}$ values began slowly to decrease indicating the start of the electrochemical reduction of the residual contaminants remained in the N4111(TFSI) after previous very careful drying at 100 °C and 10 kPa for 20 h. Steep reduction of the $C_p \cdot C_s^{-1}$ values took place at $E \leq -2.00$ V indicating the start of the intensive electrochemical reduction of N4111(TFSI) at the Al surface (Figs. 2, 3b, 4b, c). After that very steep decrease, the $C_p \cdot C_s^{-1}$ values stabilised nearly at zero ($C_p \cdot C_s^{-1} < 0.1$) at $E \leq -2.40$ V indicating the existence of very high intensity charge transfer processes at the N4111(TFSI) | Al interface (Figs. 2, 3b, 4b, c and 5b), thus, in an agreement with the XPS results discussed.

The values of series resistance (R_s) of the N4111(TFSI) | Al system were almost stable within the potential range from −2.50 to 0.00 V having an average value $R_s = 184 \pm 3$ Ω cm^2 (Fig. 6). A R_s peak ($R_s = 203$ Ω cm^2) at $E = -1.20$ V is notable, and it could be connected with the formation of non-conducting layer by electroreduction of the trace water adsorbed at the Al electrode. At $E < -2.5$ V, R_s decreases passing a minimum at -2.80 V $< E < -2.70$ V ($R_s = 174$ Ω cm^2) and started to increase again at $E < -2.80$ V obtaining a value ($R_s = 187$ Ω cm^2) that was very close to the R_s values at $E > -2.50$ V. This temporal reduction in the R_s values

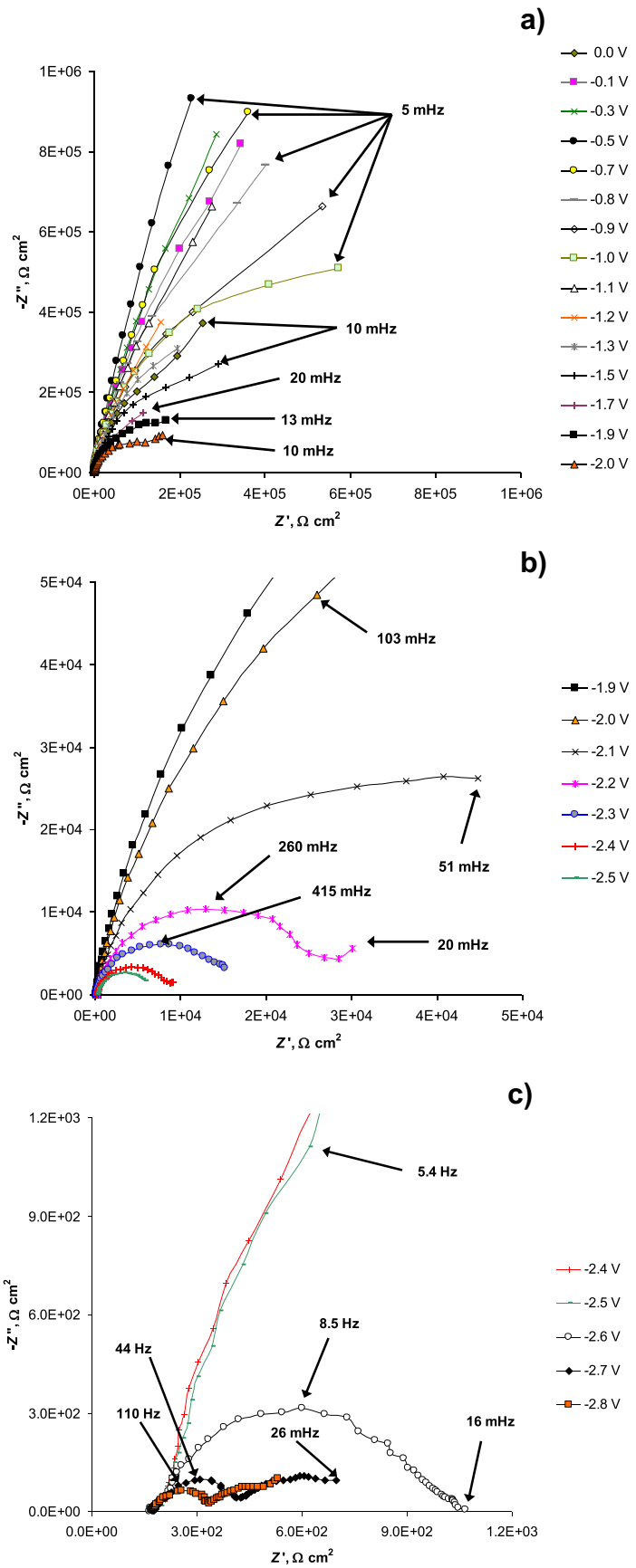

Fig. 4 **a**–**c** Nyquist plots for N4111(TFSI) | Al system measured at the potentials noted in the figure

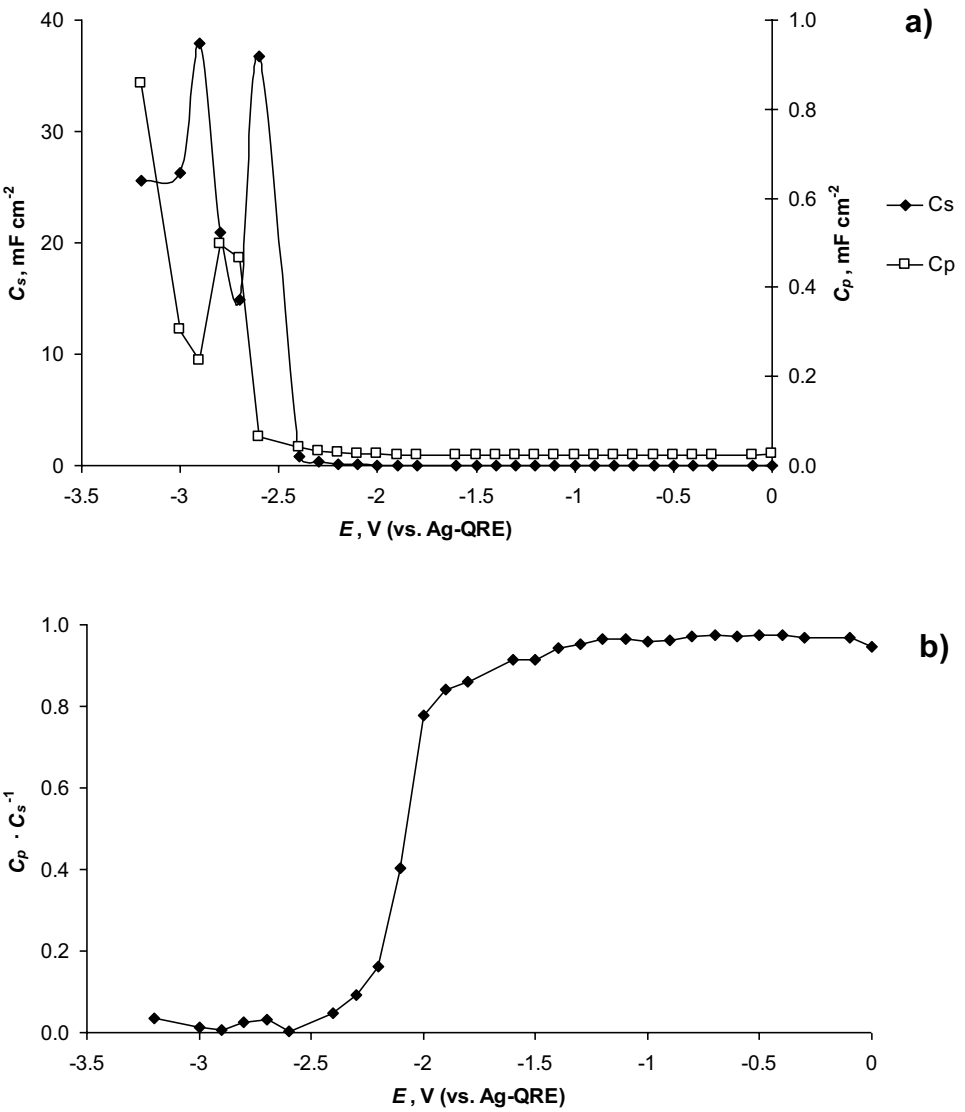

Fig. 5 Series capacitance (C_s) and parallel capacitance (C_p) (**a**) and $C_p \cdot C_s^{-1}$ (**b**) vs. Al electrode potential (E) relationships measured at the electrochemical impedance spectroscopy modulation frequency 0.10 Hz

seems to be connected with the start of the electroreduction of the $N4111^+$ cation and the formation of the gas bubbles (cleaning the surface) speeding up the mass transport at the N4111(TFSI) | Al interface [17].

The parallel resistance (R_p) increased from the initial value $R_p = 0.76$ MΩ cm^2 at $E = 0.00$ V to a peak value $R_p = 7.5$ MΩ cm^2 at $E = -0.50$ V (Fig. 6b). This R_p peak overlaps with the $C_p \cdot C_s^{-1}$ vs. E maximum ($C_p \cdot C_s^{-1} = 0.98$) at $E = -0.50$ V and marks the potential of the highest electrochemical inertness of the N4111(TFSI) interface. At more negative potentials, steep reduction in the R_p values took place; however, a small R_p peak ($R_p = 2.4$ MΩ cm^2) formed at $E = -1.10$ V indicating the possible short-term electrochemical passivation of the N4111(TFSI) | Al interface due to the electroreduction of the residual water. At $E \leq -1.20$ V continuous smooth reduction of the R_p value took place indicating the intensification of the charge transfer processes at the Al electrode surface. At $E < -2.50$ V steep increase in a parallel current density (i_p, $i_p = E \cdot R_p^{-1}$) value is notable, reflecting the start of the intensive electroreduction of the $N4111^+$ cations [17] (Fig. 6c).

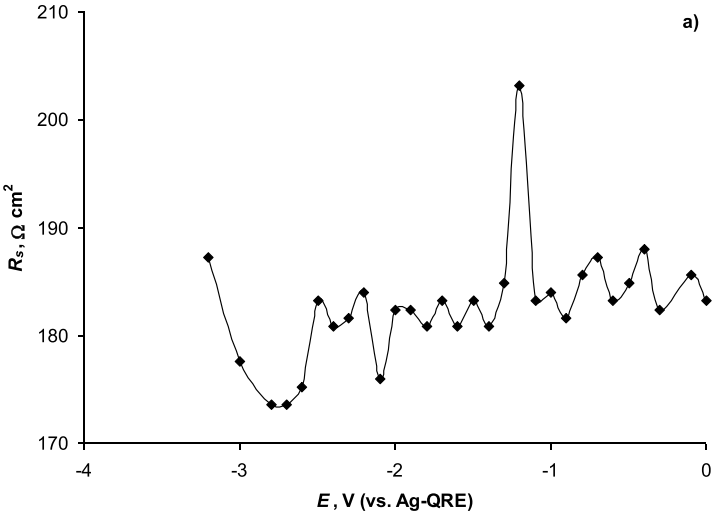

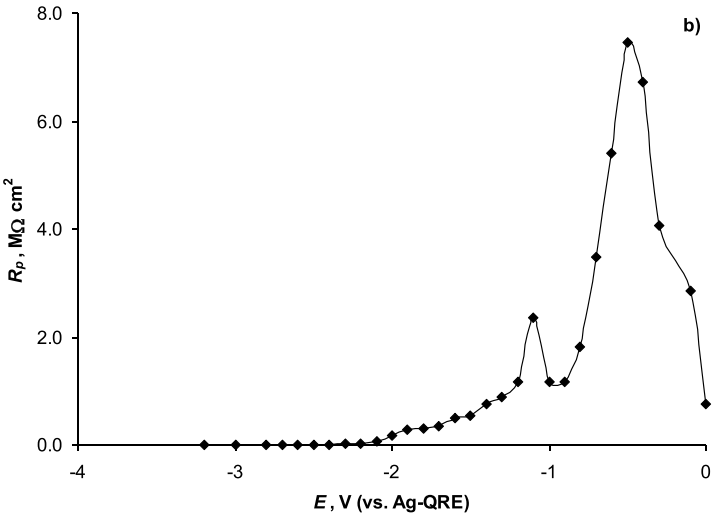

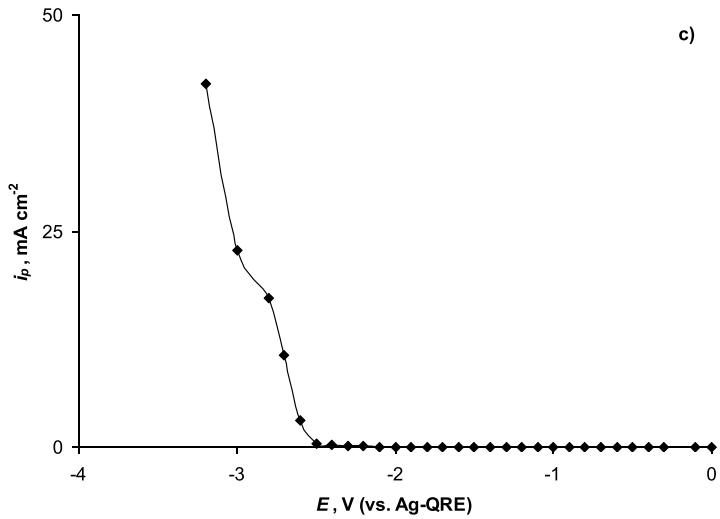

Fig. 6 Series resistance (R_s) (**a**), parallel resistance (R_p) (**b**) and parallel current density (i_p, $i_p = E \cdot R_p$) (**c**) vs. potential (E) applied for N4111(TFSI) | Al system

Conclusion

Collected in situ XPS, CV and EIS data show high electrochemical stability of the N4111(TFSI) | Al system within the potential range from −1.20 to 0.00 V (vs. Ag-QRE), where the $C_p \cdot C_s^{-1} \geq 0.97$. At more negative potentials, electrochemical reduction of trace water still remained in the N4111(TFSI) after careful drying reduced somewhat the ideal polarisability of the N4111(TFSI) | Al interface. Due to electrochemical reduction of the $N4111^+$ cations starting at $E < -2.00$ V, the $C_p \cdot C_s^{-1}$ values decrease sharply. With the start of the electroreduction of $N4111^+$ cation, the dBE vs. dE relationship slope reduced from initial value of $dBE \cdot dE^{-1} \approx -1.0$ eV V^{-1} (characteristic of the non-specific adsorption of N4111(TFSI) et al.) at $-2.25\ V < E < 0.00$ V to $dBE \cdot dE^{-1} \approx -0.6$ eV V^{-1} (corresponding to specific adsorption of N4111(TFSI) at $-3.25 < E < -2.25$ V. Within the potential range from −4.25 to −3.25 V, N4111(TFSI) adsorbed very strongly at the Al electrode surface ($dBE \cdot dE^{-1} \approx -0.1$ eV V^{-1}). The dBE vs. dE relationships are very similar for inner core electrons of all elements composing N4111(TFSI). Measured EIS and CV data are in a very good agreement with the obtained in situ XPS data, indicating the high quality of the investigation method and measurements performed.

Finally, it should be noted that the investigated N4111(TFSI) | Al system behaves very similarly to the N4111(TFSI) | mmp-C(Mo_2C) system (mmp-C(Mo_2C) denotes micro-mesoporous molybdenum carbide derived carbon electrode) [17]. However, mmp-C(Mo_2C) seems to be more active than Al, and there has been very sharp reduction of the dBE vs. dE relationship slope from the initial value of $dBE \cdot dE^{-1} \approx -1.0$ eV V^{-1} (at $-2.00\ V < E < 0.00$ V) to value $dBE \cdot dE^{-1} \approx -0.1$ eV V^{-1} in the potential range $-4.25 < E < -2.00$ V [17].

Thus, the collected data show that the application of N4111(TFSI) as an electrolyte (molten salt) for the electrochemical double layer capacitors or for the deposition of high quality metal layers of the electrochemically active metals is questionable at $E < -2.0$ V.

Supplementary Information The online version contains supplementary material available at https://doi.org/10.1007/s10008-022-05281-0.

Acknowledgements This work was supported by the EU through the European Regional Development Fund under projects TK 141 (2014-2020.4.01.15-0011), NAMUR+ (2014-2020.4.01.16-0123) and NAMUR (3.2.0304.12-0397); Estonian Research Council (PRG676 and IUT20-57); European Spallation Source: Estonian Participation in ESS Instrument design, development and building and application for scientific research (SLOKT12026T and SLTKT16432T); project "Production of Polymer Electrolyte Membrane Fuel Cell" (LLTKT20148) and project "Developing new research services and research infrastructures at MAX IV synchrotron radiation source" (2014-2020.4.01.20-0278). We acknowledge MAX IV Laboratory (University of Lund, Sweden) for time on Beamline FinEstBeAMS under Proposal 20210300. Research conducted at MAX IV, a Swedish national user facility, is supported by the Swedish Research council under contract 2018-07152, the Swedish Governmental Agency for Innovation Systems under contract 2018-04969 and Formas under contract 2019-02496. We also acknowledge Beamline FinEstBeAMS beamline manager Antti Kivimäki and research engineer Kirill Chernenko and Beamline FlexPES low density matter branch beamline manager Maxim Tchaplyguine for their very kind support.

References

1. Lane GH (2012) Electrochemical reduction mechanisms and stabilities of some cation types used in ionic liquids and other organic salts. Electrochim Acta 83:513–528. https://doi.org/10.1016/j.electacta.2012.08.046
2. Mousavi MPS, Kashefolgheta S, Stein A, Bühlmann P (2016) Electrochemical stability of quaternary ammonium cations: an experimental and computational study. J Electrochem Soc 163:H74. https://doi.org/10.1149/2.0671602jes
3. De Vos N, Maton C, Stevens CV (2014) Electrochemical stability of ionic liquids: general influences and degradation mechanisms. ChemElectroChem 1:1258–1270. https://doi.org/10.1002/celc.201402086
4. Howlett PC, Izgorodina EI, Forsyth M, MacFarlane DR (2006) Electrochemistry at negative potentials in bis(trifluoromethanesulfonyl) amide ionic liquids. Z Phys Chem 220:1483–1498. https://doi.org/10.1524/zpch.2006.220.10.1483
5. Simon P, Gogotsi Y (2008) Materials for electrochemical capacitors. Nat Mater 7:845–854. https://doi.org/10.1038/nmat2297
6. Huang Y, Li Y, Gong Q, Zhao G, Zheng P, Bai J, Gan J, Zhao M, Shao Y, Wang D, Liu L, Zou G, Zhuang D, Liang J, Zhu H, Nan C (2018) Hierarchically mesostructured aluminum current collector for enhancing the performance of supercapacitors. ACS Appl Mater Interfaces 10:16572–16580. https://doi.org/10.1021/acsami.8b03647
7. Kumar N, Pradhan L, Kumar Jena B (2022) Recent progress on novel current collector electrodes for energy storage devices: supercapacitors. WIREs Energy Environ 11:e415. https://doi.org/10.1002/wene.415
8. Jänes A, Lust E (2008) Micro– and mesoporous carbon based electrode materials for electrical double layer capacitors. ECS Transact 6:269–278. https://doi.org/10.1149/1.2943247
9. Jänes A, Thomberg T, Tõnurist K, Kurig H, Laheäär A, Lust E (2008) Micro- and mesoporous carbide-derived carbon materials and polymer membranes for supercapacitors. ECS Transact 16:57–67. https://doi.org/10.1149/1.2985627
10. Jänes A, Eskusson J, Kanarbik R, Saar A, Lust E (2012) Surface analysis of supercapacitor electrodes after long-lasting constant

current tests in organic electrolyte. J Electrochem Soc 159:A1141–A1147. https://doi.org/10.1149/2.008208jes
11. Tõnisoo A, Kruusma J, Pärna R, Kikas A, Hirsimäki M, Nõmmiste E, Lust E (2013) In situ XPS studies of electrochemically negatively polarized molybdenum carbide derived carbon double layer capacitor electrode. J Electrochem Soc 160:A1084–A1093. https://doi.org/10.1149/2.042308jes
12. Kruusma J, Tõnisoo A, Pärna R, Nõmmiste E, Lust E (2014) In situ XPS studies of electrochemically positively polarized molybdenum carbide derived carbon double layer capacitor electrode. J Electrochem Soc 161:A1266–A1277. https://doi.org/10.1149/2.0641409jes
13. Kruusma J, Tõnisoo A, Pärna R, Nõmmiste E, Tallo I, Romann T, Lust E (2016) Influence of the negative potential of molybdenum carbide derived carbon electrode on the in situ synchrotron radiation activated X-ray photoelectron spectra of 1-ethyl-3-methylimidazolium tetrafluoroborate. Electrochim Acta 206:419–426. https://doi.org/10.1016/j.electacta.2015.10.060
14. Blundell RK, Licence P (2014) Quaternary ammonium and phosphonium based ionic liquids: a comparison of common anions. Phys Chem Chem Phys 16:15278–15288. https://doi.org/10.1039/c4cp01901f
15. Campana FP, Hahn M, Foelske A, Ruch P, Kötz R, Siegenthaler H (2006) Intercalation into and film formation on pyrolytic graphite in a supercapacitor-type electrolyte $(C_2H_5)_4NBF_4$/propylene carbonate. Electrochem Commun 8:1363–1368. https://doi.org/10.1016/j.elecom.2006.06.013
16. Kurig H, Jänes A, Lust E (2010) Electrochemical characteristics of carbide-derived carbon | 1 -ethyl-3-methylimidazolium tetrafluoroborate supercapacitor cells. J Electrochem Soc 157:A272–A279. https://doi.org/10.1149/1.3274208
17. Kruusma J, Tõnisoo A, Pärna R, Thomberg T, Kook M, Romann T, Kisand V, Lust E (2021) The electrochemical behaviour of quaternary amine based room-temperature ionic liquid: N4111(TFSI) at negatively and positively polarized micro-mesoporous carbon electrodes investigated by in situ X-ray photoelectron spectroscopy, mass-spectroscopy, cyclic voltammetry and electrochemical impedance spectroscopy methods. Catalysts 11:1315. https://doi.org/10.3390/catal11111315